J. Meas. Sci. Instrum., 2025, 16(1): 96-106.
DOI: 10.62756/jmsi.1674-8042.2025010
http://jmsi.publish.founderss.cn
jmsi@nuc.edu.cn

Repetitive control without inductance decoupling for VSR control strategy of DC charging pile

LIU Peijin[1], SUN Changhe[1], HE Lin[2*], ZHANG Xiangrui[1], FENG Zhengming[1]

1. College of Mechatronics Engineering, Xi'an University of Architecture and Technology, Xi'an 710055, China;
2. College of Science, Xi'an University of Architecture and Technology, Xi'an 710055, China

***Corresponding author:** HE Lin (helin716@163.com)

Received: October 18, 2023 **Revised:** January 3, 2024 **Accepted:** January 24, 2024

Abstract: A control strategy of repetitive control without inductorance decoupling was proposed to address the problem of high total harmonic distortion (THD) rate of the network-side current caused by the reduced stability of the rectifier module of the DC charging pile under weak grid as well as the dead zone and nonlinearity of switching devices during charging. Firstly, the parallel repetitive control was constructed in the inner current loop, and the proportional-integral (PI) + repetitive controller based on parallel structure was designed. For system compensation, a second-order low-pass filter was selected to correct the system, and the network-side current harmonics were actively suppressed without increasing the filtering device, which effectively improves the quality of grid-connected current. Secondly, based on the synthetic vector method, the controller parameters were designed to realize the elimination of main pole by establishing two synchronous rotation coordinate system vector differential equations, so as to realize the inductanceless decoupling to cope with the influence of network-side inductance fluctuation on the stability of the control system under weak grid. By theoretical analysis and simulation, the proposed control strategy was embedded into the self-developed digital signal processor for the rectifier module of DC charging pile, simulated dynamic and steady-state operation experiments were conducted, and comparative analysis was performed to prove the feasibility of the proposed control strategy.

Key words: weak grid; DC charging pile; voltage source rectifier (VSR); repetitive control; inductanceless decoupling

0 Introduction

In recent years, China has been vigorously promoting the industrialization and scale development of electric vehicles and their charging facilities to achieve the goals of "double carbon" and a new type of electric power system[1]. With the gradual increase of electric vehicles, the performance and reliability of charging piles must be confronted with challenges. Compared with AC charging piles, DC charging piles have higher efficiency and faster charging speed, therefore, it has been the main development direction of charging piles[2]. Due to dispersiveness and randomness of charging loads of electric vehicles as well as dead zones and nonlinearity of switching devices, harmonics and voltage deviation may occur[3]. Additionally, since extensive and scattered large-scale renewable energy generation and distributed power sources, accompanied by long-distance transmission lines and multi-stage transformers, access to the grid, resulting in the characteristics of a weak grid and non-negligible grid equivalent inductance that affects the stability of grid-connected charging piles, therefore, it is crucial for the rectifier module of DC charging pile to suppress its grid-connected current harmonics, quickly respond to the fluctuation of grid-side inductance, operate with high power factor, and maintain the stability and robustness of DC bus voltage during charging.

In the control of the rectifier module of double closed-loop grid-connected DC charging pile, the inner current loop is often under proportional-integral (PI) control based on feed-forward decoupling, thus fast tracking the three-phase symmetric sinusoidal fundamental signal on AC side. However, its ability of suppressing periodic disturbance is poor[5], which may result in instability of the system due to incomplete decoupling of the inner current loop in case of inductance value with error or fluctuation[6]. Xiao et al. [7-9] used intelligent control methods such as adaptive and fuzzy predictive controllers to improve the performance of rectifiers. Although the

development of digital technology has accelerated the application of intelligent control in rectifier modules, it leads to an increase in the computational complexity and computational burden of conventional processors.

Repetitive control is based on internal mode principle (IMP), with better steady-state current control performance after the elimination of periodic deviations of control signals but poor dynamic performance due to the delay from repetitive control[10,11]. Jiang et al.[12] used 1/6 fundamental period repetitive control to reduce the control delay to 1/6 of the original one, which requires multiple coordinate transformations and relatively complicated control structure. Zhao et al.[13] utilized fractional phase overrun compensation to increase the gain of repetitive control, improving the error convergence rate but reducing stability of the system. Zhou et al.[14] proposed a combined control strategy with parallel repetitive control and PI control (referred to as PI+ repetitive control), achieving good current dynamic response while effectively suppressing current harmonics, without considering the impact of network-side inductance fluctuations on system performance under weak grids.

Based on this, we propose a control strategy of repetitive control combined with inductanceless decoupling, being free of the influence of inductance variation, maintaining the stable bus voltage and high power factor of the rectifier, improving the precision of inner loop current steady-state control, and effectively suppressing the current harmonics of the network. Simulation and experiment show that it is suitable for the control of DC charging pile rectifies in case of a weak grid with high percentage of renewable energy access.

1 Topological structure of DC charging pile rectifier

The topological structure of a DC charging pile rectifier is shown in Fig.1, taking a three-phase voltage source PWM rectifier (VSR) for example, where U_a, U_b, U_c and i_a, i_b, i_c are the voltages and currents of input AC side of the charging pile, respectively; L is the inductor connecting the rectifier with the grid; R is the equivalent resistor; C is the capacitor of DC side regulated filter; and R_L is the equivalent load; i_{dc} and U_{dc} are the DC bus current and voltage of the rectifier, respectively. Each bridge arm uses two sets of insulated gate bipolar transistors (IGBTs), and reverse parallel current-continuing diodes are connected at both ends to protect the circuit.

To facilitate the study, achieving the synchronous rotation of controllable variables with grid frequency up to a relative stationary state, the model in three-phase rotating synchronous abc coordinates is transformed into a mathematical model in two-phase stationary dq coordinates by Clark transform and Park transform as [15]

$$\begin{cases} L\dfrac{\mathrm{d}i_d}{\mathrm{d}t} = e_d - Ri_d - u_d^* + \omega L i_q, \\ L\dfrac{\mathrm{d}i_q}{\mathrm{d}t} = e_q - Ri_q - u_q^* - \omega L i_d, \\ C\dfrac{\mathrm{d}U_{dc}}{\mathrm{d}t} = \dfrac{3}{2}\left(i_d S_d + i_q S_q\right) - i_L, \end{cases} \tag{1}$$

where e_d and e_q are the active and reactive voltage components in dq coordinates, respectively; and i_d and i_q are the active and reactive current components in dq coordinates, respectively. The dual closed-loop control structure with outer voltage loop and inner current loop is adopted. The outer voltage loop controls the voltage output on the DC side following the given voltage quickly, while the inner current loop controls the current input on AC side being sinusoidal and synchronized with the grid voltage so as to track the commanded current.

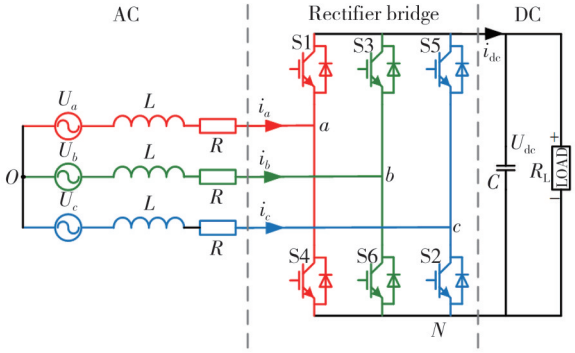

Fig. 1 Topological structure of three-phase AC/DC rectifier

2 Inner loop current control strategy

In this study, repetitive control in parallel with PI control is combined with inductanceless decoupling to form a new inner loop current control strategy applied to the rectifier of DC charging pile, as shown in Fig.2.

The traditional PI control of inner loop current can be designed in a closed loop form, as shown in Fig.3.

In Fig. 3, $G_{PI}(s)$ is the PI controller for inner loop current, $G_D(s)$ is the time delay, $G_P(s)$ is the controlled object, i_x is the disturbance signal, i_{dq}^* is the current command value in dq coordinates obtained from the outer loop voltage, and i_{dq} is the output current. As we know, dq coordinates indicate d-axis (active) and q-axis (reactive) currents. In fact, to achieve a power factor close to 1, reactive current i_q must be zero. For further analysis, inner loop currents are $i_{dq}^* = i_d^*$ and $i_{dq} = i_d$.

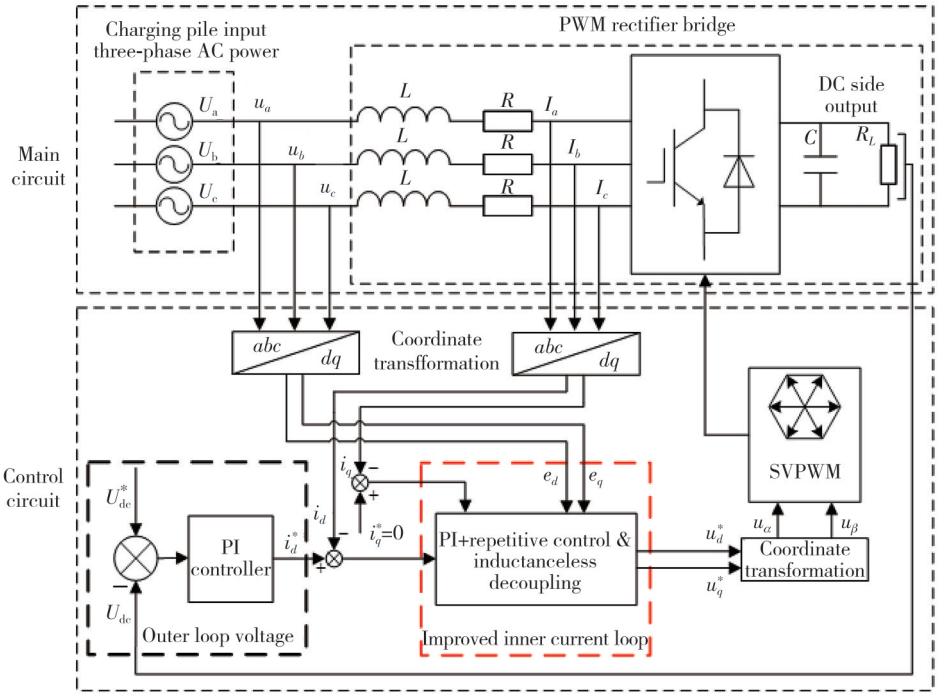

Fig. 2 Control structure of rectifier

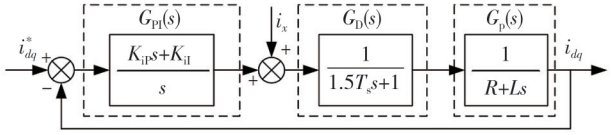

Fig. 3 Control structure of inner loop current

To improve the ability to suppress the harmonics of the rectifier, a PI+repetitive controller with a parallel structure is designed. The controller is eventually digitized for analysis in the discrete domain[16]. As shown in Fig. 4, $G_{RC}(z)$ is the repetitive controller, $G_{PD}(z)$ is the system function of the internal model and the delay, and $G_{PIRC}(z)$ is the system function of the PI+repetitive controller. For convenience, interference signal i_x is equivalently transferred to the output side of $G_{PD}(z)$[17].

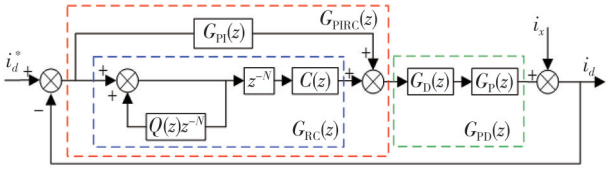

Fig. 4 PI+repetitive control structure for inner loop current

The repetitive controller is expressed as

$$G_{RC}(z)=\frac{k_r z^{-N+k}S(z)}{1-Q(z)z^{-N}}, \tag{2}$$

where $N=\dfrac{f_s}{f}$ is the number of sampling points per cycle for repetitive control, f_s is the switching frequency, and f is the frequency of three-phase voltage; z^{-N} is the cycle delay, taking the current cycle error as the corrected quantity for the next cycle; and $Q(z)$ is the internal model coefficient. An ideal model of repetitive control has N open-loop poles in discrete domain, resulting in critical stability of the system, while $Q(z)$ can enhance the robustness of the repetitive control, here $Q(z)=0.95$. The Byrd diagram of the repetitive signal generator $\dfrac{1}{1-Q(z)z^{-N}}$ is shown in Fig. 5, which presents high gain at an integer multiple of the fundamental frequency of 50 Hz, meaning that the improved repetitive controller can effectively suppress periodic interference and follow the periodic given signal.

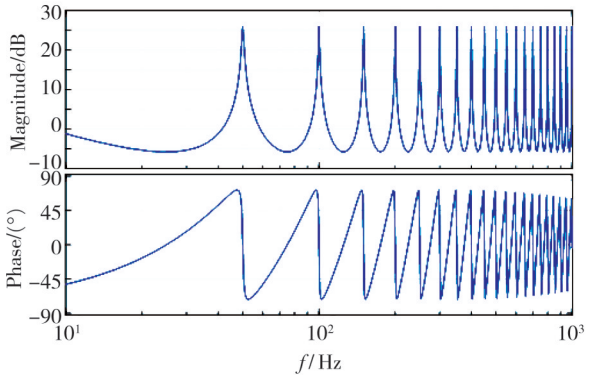

Fig. 5 Byrd diagram of improved repetitive signal generator

In Eq. (2), $C(z)$ is for compensation, correcting the amplitude and phase of the low-frequency signal of the system while attenuating the high-frequency interference signal. $C(z)=k_r z^k S(z)$, where k_r is the scaling factor, controlling a reasonable match between the stability margin and the error convergence rate, which is known to be the fastest at $k_r=1$[18]; z^k is to compensate for the

phase lag in the low and medium frequency bands, with $k=3$ after simulation and experimental verification; $S(z)$ is to correct the system by using the second-order low-pass filter, that attenuates the low frequency signal to 0 and the high-frequency signal rapidly to cut the unwanted high-frequency signal off. A cutoff frequency of 1 kHz and a damping factor of 0.707 are chosen to obtain the discrete domain system function as

$$S(z)=\frac{0.067\,45+0.134\,9z^{-1}+0.067\,45z^{-2}}{1-1.142\,98z^{-1}+0.412\,8z^{-2}}. \quad (3)$$

The Byrd diagram of Eq. (3) is shown in Fig.6. It can be seen that the high-frequency signal is effectively attenuated.

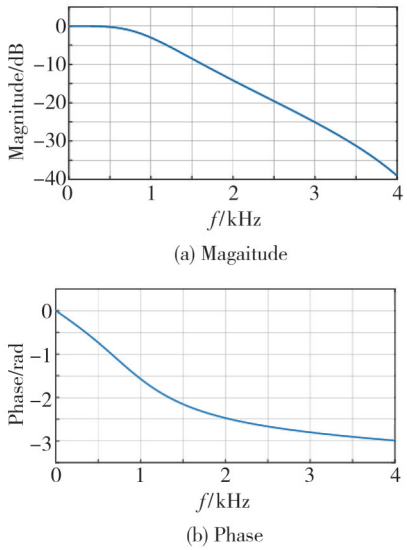

Fig. 6 Byrd diagram of filter $S(z)$

$G_{PI}(z)$ is the system function of the PI controller in the discrete domain, and its mathematical expression is

$$G_{PI}(z)=K_{iP}+K_{iI}z/(z-1). \quad (4)$$

The PI control in parallel with repetitive control is expressed as

$$G_{PIRC}(z)=G_{PI}(z)+G_{RC}(z). \quad (5)$$

The current closed-loop system function is

$$G_H(z)=\frac{i_d(z)}{i_d^*(z)}=\frac{G_{PD}(z)G_{PIRC}(z)}{1+G_{PD}(z)G_{PIRC}(z)}. \quad (6)$$

Thus, the characteristic equation can be expressed as

$$1+G_{PD}(z)G_{PIRC}(z)=0. \quad (7)$$

Substituting Eq. (2) into Eq. (7), we can get

$$\left[1+G_{PI}(z)G_{PD}(z)\right]\times \left\{1-z^{-N}\left[Q(z)-C(z)G_W(z)\right]\right\}=0, \quad (8)$$

where G_W is the current closed-loop system function of the repetition-free controller, which is expressed as

$$G_W(z)=\frac{G_{PD}(z)}{1+G_{PI}(z)G_{PD}(z)}. \quad (9)$$

For PI+repetitive control structure, the sufficient conditions for system stability are: 1) The poles of the closed-loop system function, namely all solutions of the characteristic equation, lie within the unit circle, and the PI control is stabilized by choosing the roots of $G_W(z)$; 2) According to small gain theorem[19], let $z=e^{j\omega T}$, the stability of the repetitive control can be obtained by

$$\left|Q(e^{j\omega T})-C(e^{j\omega T})G_W(e^{j\omega T})\right|<1,\ \omega\in\left[0,\frac{\pi}{T}\right], \quad (10)$$

where T is the sampling period.

Let $H(e^{j\omega T})=Q(e^{j\omega T})-C(e^{j\omega T})G_W(e^{j\omega T})$. On the premise that PI control is stable, the internal model coefficient $Q(e^{j\omega T})=0.95$, which shifts the unit circle left and makes $H(e^{j\omega T})$ lie within the full frequency band, thus the whole system is stable under the action of the compensation $C(e^{j\omega T})$, as shown in Fig.7.

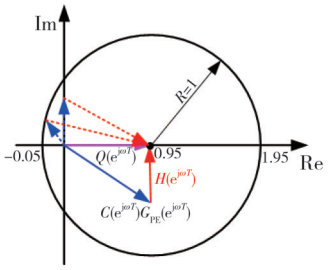

Fig. 7 Stability analysis of repetitive control

3 Inductanceless decoupling

In Eq. (1), there are coupling terms: ωLI_q and ωLI_d. Since the rectifier of the DC charging pile generally adopts the traditional feed-forward decoupling control, for PI+ repetitive control, we can get

$$\begin{cases} U_d^*=-G_{PIRC}(z)\left(I_d^*-I_d\right)+E_d+\omega LI_q, \\ U_q^*=-G_{PIRC}(z)\left(I_q^*-I_q\right)+E_d-\omega LI_d. \end{cases} \quad (11)$$

Subsequently, the exact value of inductance L needs to be known. Since the coupling between d and q axes is enhanced with the increase of frequency, the fluctuation of inductance value will affect the control performance of the rectifier. When a DC charging pile is connected to the grid, the grid-side filter inductance L of the rectifier will be in series with the larger grid equivalent inductance L_g of weak grid, causing the grid-connected rectifier to be destabilized[20]. Therefore, the inductanceless decoupling method based on PI+repetitive control is proposed.

The vector model of the rectifier in the two-phase stationary $\alpha\beta$ coordinates is derived from its mathematical model in three-phase abc coordinates as[21]

$$L\frac{d\boldsymbol{I}_{\alpha\beta}}{dt}+R\boldsymbol{I}_{\alpha\beta}=\boldsymbol{E}_{\alpha\beta}-\boldsymbol{U}_{\alpha\beta}, \quad (12)$$

where $\boldsymbol{I}_{\alpha\beta}$ is the synthetic vector of the input current,

$\boldsymbol{E}_{\alpha\beta}$ is the synthetic vector of the input voltage, and $\boldsymbol{E}_{\alpha\beta}$ is the synthetic vector of the control voltage.

Eq. (12) is transformed from $\alpha\beta$ coordinates into synchronously rotating dq coordinates with $\frac{\mathrm{d}}{\mathrm{d}t}$ replaced by differential operator $\frac{\mathrm{d}}{\mathrm{d}t}+\mathrm{j}\omega$, that is

$$\left(\frac{\mathrm{d}}{\mathrm{d}t}+\mathrm{j}\omega\right)L\boldsymbol{I}_{dq}+R\boldsymbol{I}_{dq}=\boldsymbol{E}_{dq}-\boldsymbol{U}_{dq}. \tag{13}$$

After consolidation and simplification, we can get

$$\frac{\mathrm{d}}{\mathrm{d}t}L\boldsymbol{I}_{dq}+(\mathrm{j}\omega L+R)\boldsymbol{I}_{dq}=\boldsymbol{E}_{dq}-\boldsymbol{U}_{dq}. \tag{14}$$

A Laplace transform of Eq. (14) yields

$$\boldsymbol{I}_{dq}=\frac{\boldsymbol{E}_{dq}-\boldsymbol{U}_{dq}}{L\left[s+\left(\frac{R}{L}+\mathrm{j}\omega\right)\right]}. \tag{15}$$

It can be seen that the introduction of synthetic vectors transforms the PWM rectifier from a second-order system with two inputs and two outputs to a first-order system with a single input and a single output, and the only main pole point of the system is $-R/L-\mathrm{j}\omega$. Then, the zero point of the controller, $-K_{\mathrm{iI}}/K_{\mathrm{iP}}-\mathrm{j}\omega$, is constructed to eliminate the main pole point of the system. Finally, $R/L=K_{\mathrm{iI}}/K_{\mathrm{iP}}$ is reserved, and decoupling is completed. During the programming, to optimize the program structure and reasonably allocate the system resources, the programs with high real-time performance are allocated to the interrupt program, and the others are allocated to the main program. The interrupt program is responsible for data acquisition and operation of the rectifier as well as the elimination of main pole by adjusting the inner loop current and parameters K_{iI} and K_{iP} in the program.

As for PI control, there is

$$\boldsymbol{U}_{dq}=\boldsymbol{E}_{dq}-G_{\mathrm{PI}}(z)\left(\boldsymbol{I}_{dq}^{*}-\boldsymbol{I}_{dq}\right). \tag{16}$$

Then, the control equation without inductance decoupling is obtained by PI+repetitive control as

$$\begin{cases}U_{d}^{*}=-G_{\mathrm{PIRC}}(z)\left(I_{d}^{*}-I_{d}\right)+E_{d}+\dfrac{\omega K_{\mathrm{iP}}z}{z-1}\left(I_{q}^{*}-I_{q}\right),\\ U_{q}^{*}=-G_{\mathrm{PIRC}}(z)\left(I_{q}^{*}-I_{q}\right)+E_{q}-\dfrac{\omega K_{\mathrm{iP}}z}{z-1}\left(I_{d}^{*}-I_{d}\right).\end{cases} \tag{17}$$

The comparison of Eq. (11) with Eq. (17) shows that the decoupling terms ωLI_q and ωLI_d in the original equation are replaced by $\omega K_{\mathrm{iP}}\left(I_q^{*}-I_q\right)z/(z-1)$ and $\omega K_{\mathrm{iP}}\left(I_d^{*}-I_d\right)z/(z-1)$, respectively, and the controller no longer contains inductance L, which means that the fluctuation of inductance value has no effect on the controller, and the inner loop current is completely decoupled without inductance L.

The inner loop current control structure based on PI+repetitive control without inductance decoupling is shown in Fig.8.

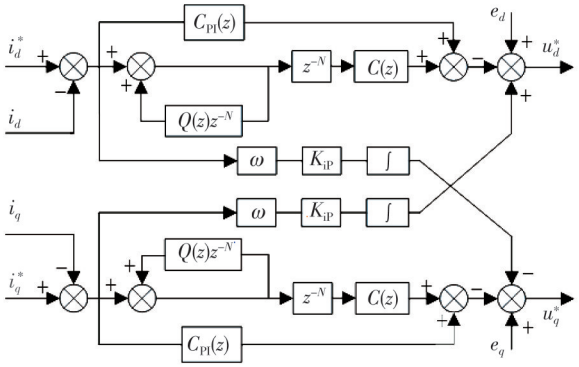

Fig. 8 Improved inner loop current control structure

4 Simulation

The simulation model of the rectifier of the DC charging pile was built using Matlab/Simulink for system performance evaluation. The simulation parameters are listed in Table 1.

Table 1 Simulation parameters of rectifier

Parameter	Value
AC-side inductance L/mH	3
DC-side capacitance C/μF	2 350
Load R_{L}/Ω	30
Input voltage U_{e}/V	380
Grid frequency f/Hz	50
Given value of DC voltage U_{dc}^{*}/V	600
Switching frequency f_{s}/kHz	10

4.1 Steady-state performance

Simulation was carried out. Fig. 9 shows the steady-state waveforms and total harmonic distortions (THDs) of network-side a-phase current of the rectifier using the traditional feed-forward decoupled PI control of inner loop current and the inductanceless decoupled PI+repetitive control of inner loop current, respectively.

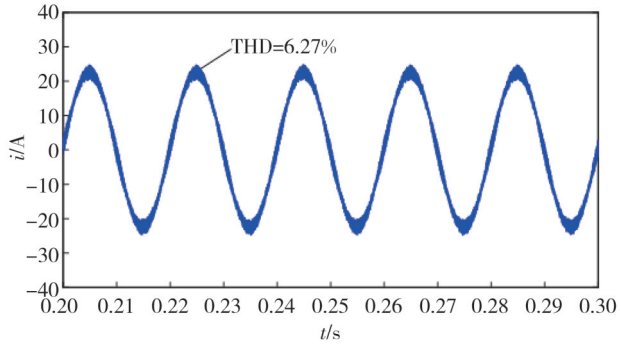

(a) A-phase current simulation waveform under PI control

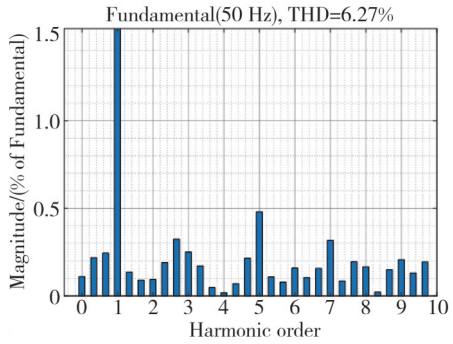

(b) A-phase current THD under PI control

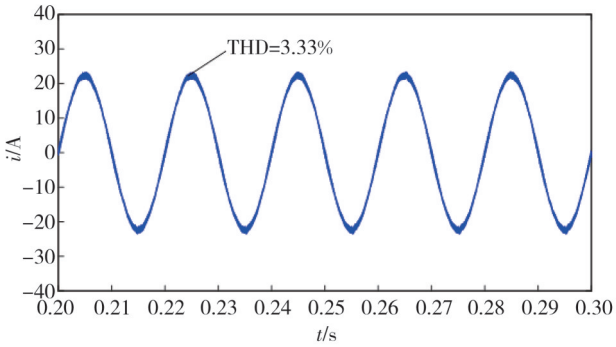

(c) A-phase current simulation waveform under improved current control

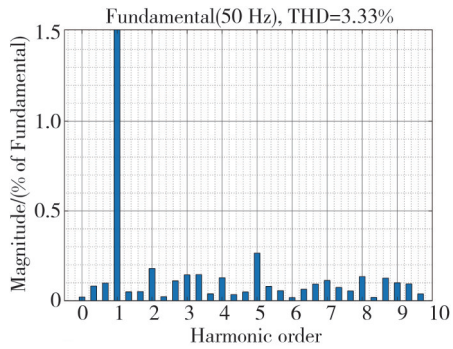

(d) A-phase current THD under improved inner loop current control

Fig. 9 A-phase current simulation waveforms and steady-state THDs

It can be seen from Fig.9 that compared with the steady-state THD of a-phase current on network-side at 50 Hz under traditional PI control, there is an improvement of 2.94% by the improved current control, meaning that the quality of network-side current waveform is significantly improved by PI+repetitive control combined with inductanceless decoupling strategy.

4.2 Dynamic robustness

4.2.1 Start-up response

From Fig.10, it can be seen that the error signals of PI control under traditional feedforward decoupling and PI+repetitive control current loop based on inductorless decoupling can both stabilize at a faster rate, and the traditional current inner loop control produces a fluctuation from −12 V to 32.5 A before the i_{derr} reaches steady state, and the i_{derr} stays between −2 A and 2 A after reaching steady state; after using the improved current inner loop control, its error is significantly reduced before the After using the improved current inner-loop control, the error is significantly reduced before reaching steady state, and the i_{derr} remains between ±0.5 A after reaching steady state, which fully reflects the good steady-state characteristics of the proposed control strategy and the more accurate control effect on periodic error signals.

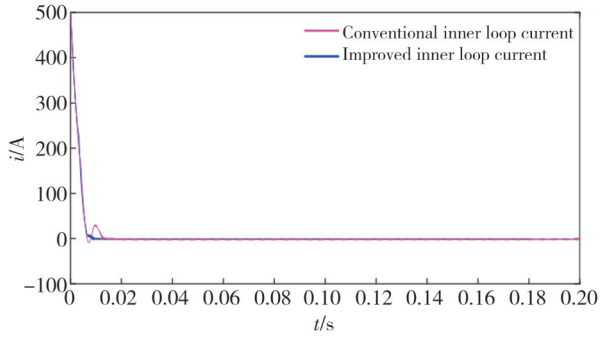

(a) Overall response curve

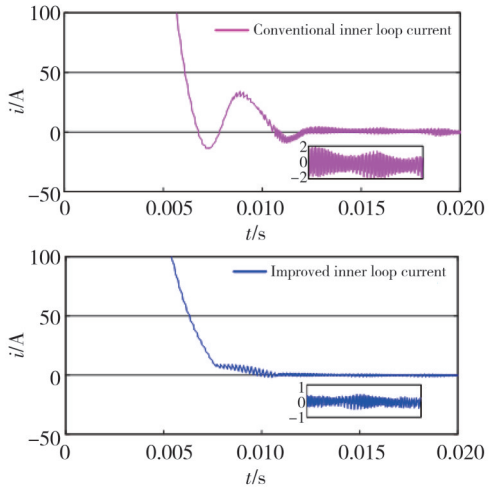

(b) Local magnification diagram

Fig. 10 Error signal of inner loop current

4.2.2 Dynamic response of inductance value change

The changes in DC-side voltage and a-phase current induced by sudden inductance value change are shown in Fig.11.

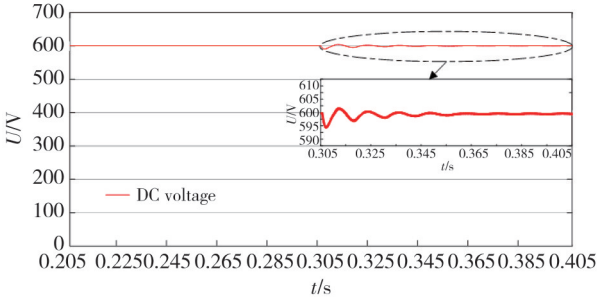

(a) Conventional inner loop current

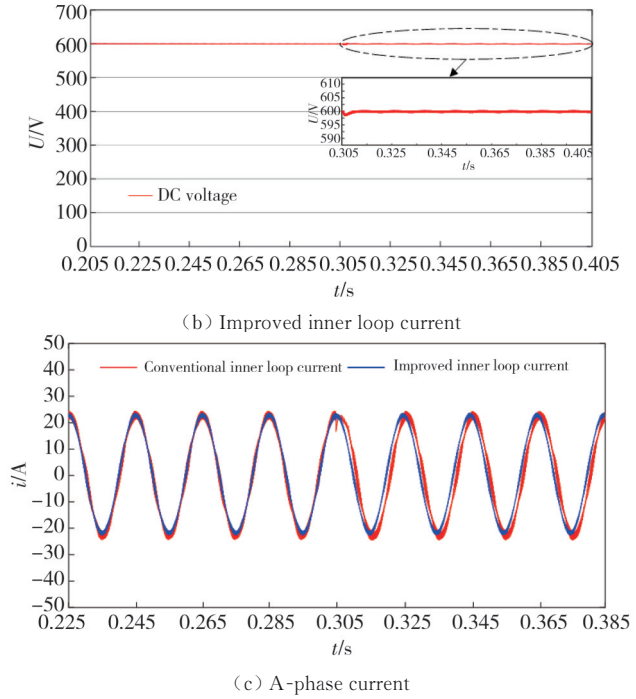

Fig. 11 DC-side voltage and a-phase current under sudden inductance value change

Fig. 11(a) shows the dynamic response of the conventional inner loop current under the sudden change of inductance value. At 0.305 s, the inductor changes abruptly from 3 mH to 6 mH, and the DC bus voltage subsequently fluctuates by 6 V, and then returns to stability after 40 ms. Fig.11(b) shows the improved inner loop current control. It can seen that the DC bus voltage fluctuates slightly by 1 V instantaneously after the sudden change of inductance value, basically eliminating the effect of inductor parameter change on the system. Fig. 11(c) shows that under the conventional inner loop current control, the AC-side current produces a dip of about 4 A at the moment of abrupt change, while the phase shows hysteresis, which leads to the reduction of the system power factor. The improved inner loop current control keeps the a-phase current and phase basically unchanged when the inductance value changes abruptly, and the system maintains unit power factor operation.

5 Experimental verification

To further verify the feasibility of the control strategy proposed in this study, the rectifier experimental platform was built on the basis of theoretical analysis and simulation verification, as shown in Fig.12, and the control algorithm was implemented by DSP28335 digital controller to test the performance of the developed rectifier module.

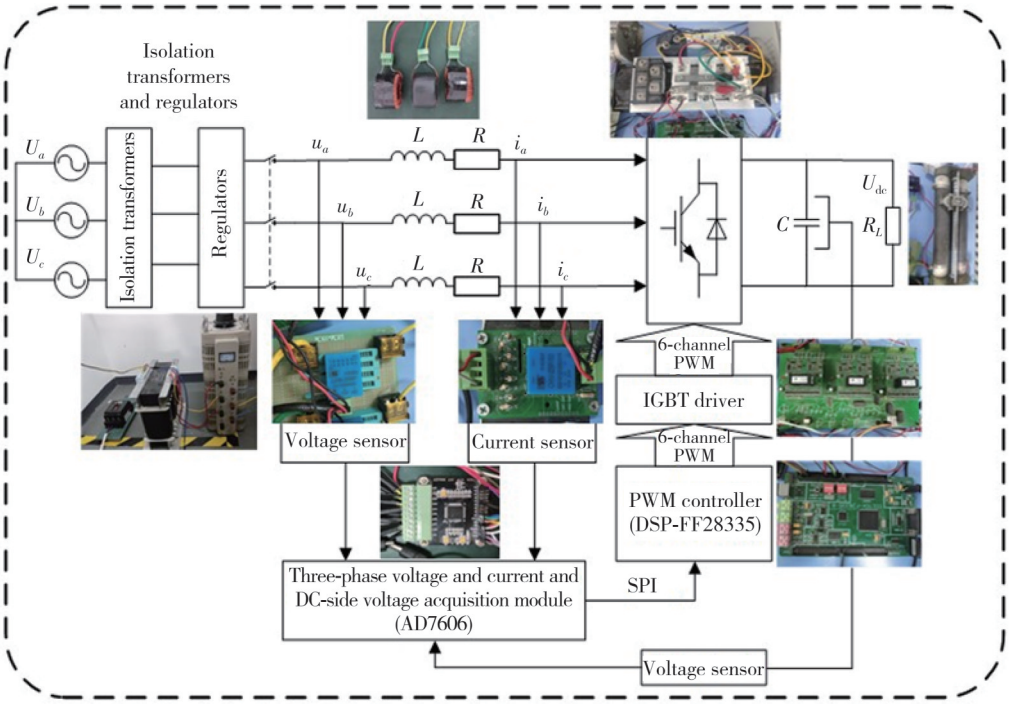

Fig. 12 Experimental system structure for performance test on rectifier module

5.1 Steady-state operation experiment

The experiments of conventional inner loop current control and improved inner loop current control at the grid frequency of 50 Hz were conducted. The a-phase output current experimental waveform and steady-state THD are shown in Fig.13.

It can be seen that when the grid frequency is 50 Hz, the ripple of the a-phase output current sinusoidal waveform under the traditional inner current PI control is more serious

and sinusoidal characteristics are poor, while the sinusoidal shape of a-phase output current under the improved inner loop current control is significantly improved, thus verifying the conclusion that the repetitive control combined with inductanceless decoupling strategy can effectively suppress the network-side harmonics.

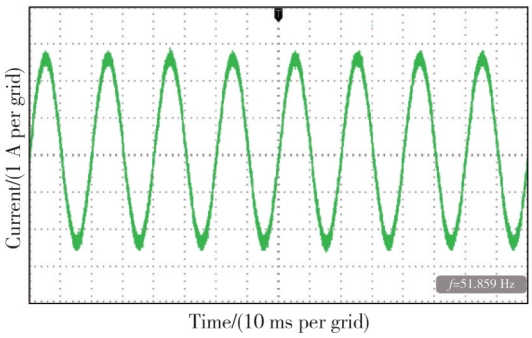

(a) A-phase current experimental waveform under PI control

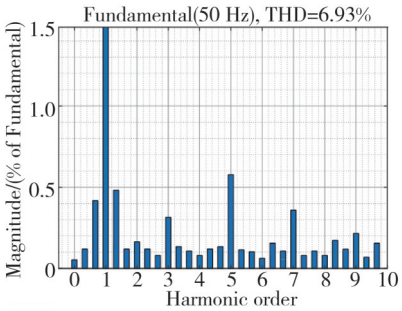

(b) A-phase current THD under PI control

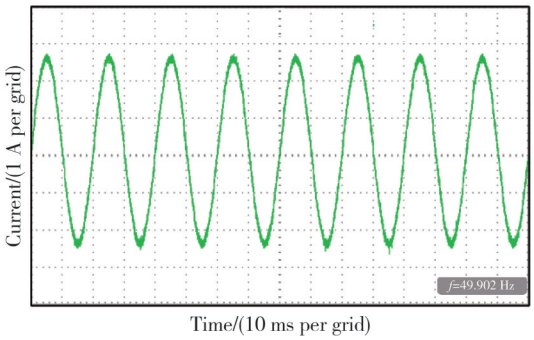

(c) A-phase current experimental waveform under improved current control

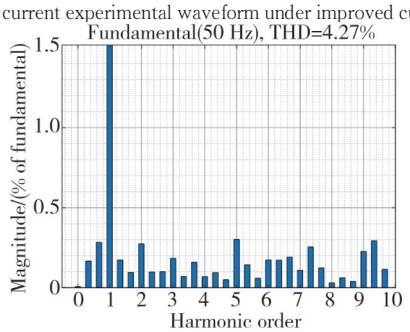

(d) A-phase current THD under improved current control

Fig. 13 A-phase current experimental waveform and steady-state THD

It also can be observed that when the grid frequency is 50 Hz, a-phase output current THD=6.93% under conventional PI control, while THD=4.27% under the improved inner loop current control, which meets the requirement of the national standard "*Power Quality Public Grid Harmonics*"[22] (GB/T145949—1993) of below 5%. Compared with the simulation results, the harmonic distortion rate THD by experiment has a small increase, which is mainly caused by the errors existing in the experimental process.

5.2 Inductance variation experiment

In order to analyze the stability of the rectifier module under weak grid, the condition of grid impedance fluctuation during charging was simulated by inductance mutation. Figs.14 and 15 show the waveforms observed by the oscilloscope when the inductance value changes abruptly under different control methods.

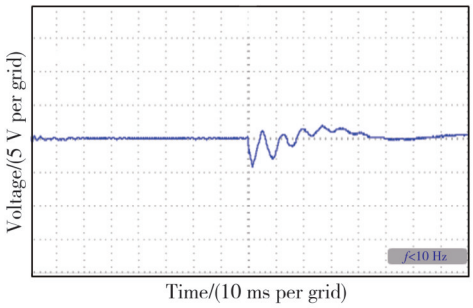

(a) DC bus voltage waveform

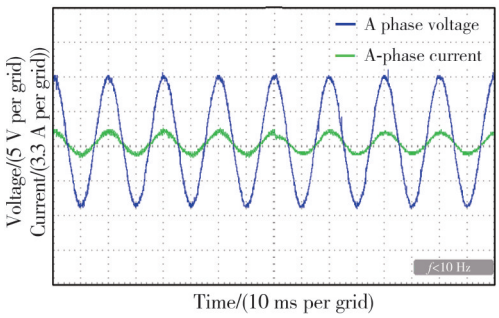

(b) A-phase current and voltage waveform

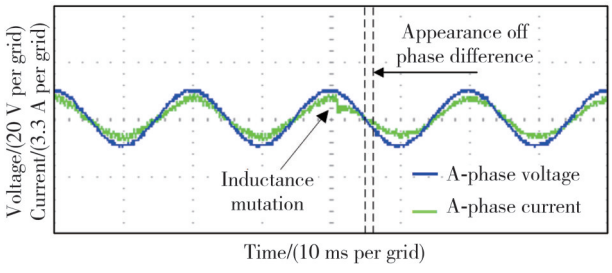

(c) A-phase current and voltage amplification waveform

Fig. 14 Experimental waveform under traditional inner loop current control

Fig.14(a) shows that under the traditional feedforward decoupled PI control of inner loop current, the DC bus voltage fluctuates by 6.2 V when the inductance value changes abruptly and then returns to stability after 44 ms. From Fig.14(b) — (c), it can be seen that the a-phase

current fluctuates under the traditional inner loop current control after the inductance value changes abruptly and produces a phase difference with the voltage, which leads to a lower power factor of the rectifier.

Fig. 15(a) shows that under the improved inner loop current control proposed in this study, the DC-side voltage produces a small fluctuation of 1.2 V when the inductance value changes abruptly. From Fig. 15(b) — (c), it can be seen that the improved inner loop current control keeps the a-phase current in phase with the a-phase voltage after the sudden inductance value change, and basically maintains the operating condition of unit power factor, which verifies that the control strategy of repetitive control combined with inductanceless decoupling has better resistance to disturbance.

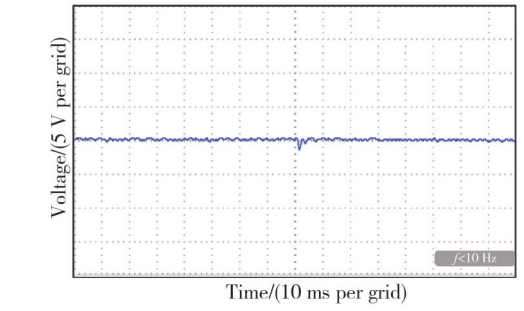

(a) DC bus voltage waveform

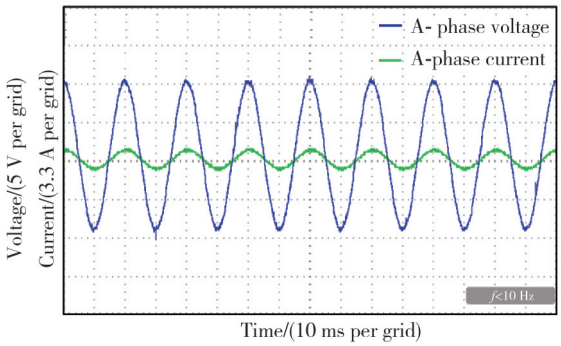

(b) A-phase current and voltage waveform

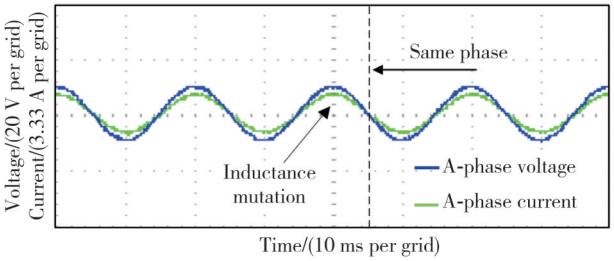

(c) A-phase current and voltage amplification waveform

Fig. 15 Improved waveform of inner loop current control experiment

6 Discussion

The Simulink simulation results are well verified in the experiments, but there are some deviations between them. For example, the steady-state experimental results show a small increase in THD compared to the simulation results, and the dynamic experimental results show a slightly larger DC current fluctuation compared to the simulation results when the inductance value changes abruptly. The reason is that the simulation is performed under ideal conditions, while the experiment is performed under non-ideal conditions with certain errors, perturbations, different degrees of nonlinearity, and the existence of three-phase grid voltage imbalance in the experiment.

7 Conclusions

In this study, for the control of DC charging pile rectifier module under weak grid effect, a control strategy of introducing repetitive control combined with inductanceless decoupling to the inner loop current was proposed, the corresponding controller design and development were carried out, and the main conclusions were verified by simulation and experiment. Compared with the traditional inner loop current control, the ripple of the output current sinusoidal waveform under the improved inner loop current control is significantly improved with THD=4.27% by experiment, which satisfies the national standard "*Power Quality Public Grid Harmonics*"[22] (GB/T145949 — 1993) requirement of less than 5%. In weak grid effect experiments, for the traditional inner loop current contol, current fluctuations due to sudden change of inductance value, lead to the reduction of power factor of the rectifier. Under the improved inner loop current control, the current remains in phase with the phase voltage and is basically in the operating state of unit power factor. Therefore, the steady-state performance, immunity and robustness of the control system are improved.

Acknowledgement

This work was supported by National Natural Science Foundation of China (No. 61903291), and Shaanxi Province Key R&D Program (No.2022GY-134).

Declaration of conflicting interests

The authors have no conflict of interests related to this publication.

References

[1] LIU W, WANG C L, XIAO T, et al. AMI data-driven state evaluation method for measurement and operation error of electric vehicle charging facilities. Electric Power

Automation Equipment, 2022, 42(10): 70-76.
[2] XU Z. Study on the performance of three phase rectifier used in electric vehicle charging pile. Modern Information Technology, 2018, 2(1): 48-50.
[3] CHENG S, WANG X N, FENG Y C. Decentralized optimization of ordered charging scheduling in electric vehicle charging station. Automation of Electric Power Systems, 2018, 42(1): 39-46.
[4] LIU Y F, ZHOU X P, CHEN Y D, et al. Sequence impedance modeling and stability analysis for load converters with inertial support. IEEE Transactions on Power Electronics, 2020, 35(12): 13031-13041.
[5] ZHAO L M, LI H F. Research of grid-connected rectifier based on the PI and repetitive control. Electric Drive, 2017, 47(2): 24-28.
[6] ZHANG Z B, WANG H Y, WANG W Q. Control strategy of electric vehicle bidirectional converter considering saturation characteristics. Science Technology and Engineering, 2022, 22(2): 577-584.
[7] XIAO X, ZHANG Y J, WANG J, et al. PWM rectifiers based on adaptive sliding-mode observer with virtual flux orientation under non-line voltage sensors control. Transactions of China Electrotechnical Society, 2015, 30(12): 152-161.
[8] YU C S, ZHANG Y. Fuzzy adaptive control strategy of voltage outer loop for single-phase PWM rectifier. Journal of Hebei University of Science and Technology, 2020, 41(1): 23-30.
[9] LÜ W J, CHU J W, WU J, et al. Investigation of a VSC-HVDC adaptive control strategy based on the model prediction strategy. Journal of Electric Power Science and Technology, 2020, 35(1): 122-129.
[10] LIN H Y, GUO X, CHEN D D, et al. A frequency adaptive repetitive control for active power filter with 380V/75A SiC-inverter. IEEE Transactions on Industry Applications, 2022, 58(4): 5469-5479.
[11] ZHANG Q, CAI F H, HUANG L M, et al. PI+repetitive control of single-phase programmable current source. Transactions of China Electrotechnical Society, 2019, 34(S1): 163-170.
[12] JIANG S, CAO D, LI Y, et al. Low-THD, fast-transient, and cost-effective synchronous-frame repetitive controller for three-phase UPS inverters. IEEE Transactions on Power Electronics, 2011, 27(6): 2994-3005.
[13] ZHAO Q S, YE Y Q, XU G F, et al. Application of improved repetitive control scheme to inverter with low sampling frequency. Transactions of China Electrotechnical Society, 2015, 30(19): 120-127.
[14] ZHOU J, REN G Y, WEI C, et al. Harmonic analysis of electric vehicle AC charging spot and research on harmonic restriction. Power System Protection and Control, 2017, 45(5): 18-25.
[15] DING Q, WANG F W, JIAO Z, et al. Simulation research of three-phase VSR based on A feed-forward control strategy in stationary coordinate system//2021 IEEE 2nd International Conference on Information Technology, Big Data and Artificial Intelligence, December 17-19, 2021, Chongqing, China. New York: IEEE, 2021: 793-798.
[16] ZHAO Q S, CHEN S S, ZHOU X Y, et al. Analysis and design of combination controller based on repetitive control and proportional control for harmonics suppression of grid-tied inverters. Transactions of China Electrotechnical Society, 2019, 34(24): 5189-5198.
[17] ALI M S, WANG L, ALQUHAYZ H, et al. Performance improvement of three-phase boost power factor correction rectifier through combined parameters optimization of proportional-integral and repetitive controller. IEEE Access, 2021, 9: 58893-58909.
[18] WANG S E, GOU Y K, HAO P F, et al. Three phase VIENNA rectifier frequency adaptive fast repetitive control strategy. Chinese Journal of Electron Devices, 2020, 43(6): 1266-1272.
[19] SONG X F, YU G K, MENG G J, et al. Design of grid-connected inverter based on improved repetitive control and fuzzy PI self-tuning. Renewable Energy Resources, 2020, 38(2): 245-251.
[20] YANG S D, LI W, ZHANG X W, et al. A virtual-impedance based control strategy for improving the adaptability of converter to weak grid. Journal of Power Supply, 2021: 1-14.
[21] CHEN Y J, ZHONG Y P. Study on the current control for voltage-source PWM rectifier using complex vectors. Proceedings of the CSEE, 2006, 26(2): 143-148.
[22] National Technical Committee for Standardization of Voltage and Current Level and Frequency. Harmonics of quality utility grid: GB/T 14549-93. Beijing: China Standards Press, 1993.

重复控制结合无电感参数解耦的直流充电桩VSR控制策略

刘沛津[1], 孙长贺[1], 何　林[2*], 张香瑞[1], 冯正明[1]

1. 西安建筑科技大学 机电工程学院, 陕西 西安 710055;
2. 西安建筑科技大学 理学院, 陕西 西安 710055

摘　要：针对直流充电桩整流模块在弱电网下稳定性降低，充电过程中开关器件死区和非线性等导致的网侧电流总谐波畸变率较高的问题，提出了重复控制结合无电感参数解耦方法的电压型整流器（Voltage source rectifier，VSR）控制策略。首先，在内环电流构造并联重复控制，设计了基于并联结构的比例积分控制（Proportional-integral，PI）＋重复控制器，并针对补偿环节，选取二阶低通滤波器对系统进行校正，在不增加滤波装置的情况下，主动抑制网侧电流谐波，有效提高并网电流质量。其次，基于合成矢量法，建立两相同步旋转坐标系矢量微分方程，设计控制器参数进行主极点对消，从而实现无电感参数解耦，以应对弱电网下网侧电感波动对控制系统稳定性的影响。在理论分析和仿真实验的基础上，将所提出的控制策略嵌入自主开发的直流充电桩整流模块数字信号处理器，模拟动态和稳态运行实验，并进行对比分析。实验结果证明了该控制策略的可行性。

关键词：弱电网；直流充电桩；电压型整流器；重复控制；无电感解耦

引用格式：LIU Peijin, SUN Changhe, HE Lin, et al. Repetitive control without inductance decoupling for VSR control strategy of DC charging pile. Journal of Measurement Science and Instrumentation, 2025, 16(1): 96-106. DOI: 10.62756/jmsi.1674-8042.2025010